Skew Incidence Plane-Wave Scattering From 2-D Dielectric Periodic Structures: Analysis by the Mortar-Element Method

(Article begins on next page)

19 April 2024

Skew Incidence Plane-Wave Scattering From 2-D Dielectric Periodic Structures. Analysis by the Mortar-Element Method.

Alberto Tibaldi, *Graduate Student Member, IEEE,* Renato Orta, *Senior Member, IEEE,*
Oscar Antonio Peverini, *Member, IEEE,* Giuseppe Addamo, Giuseppe Virone
and Riccardo Tascone, *Member, IEEE*

Abstract—A full-wave simulator of 2-D dielectric periodic structures under skew plane wave incidence is presented in this paper. A differential formulation is used and the boundary value problem is solved by means of a multi-domain spectral method. Suitable mappings allow the efficient analysis of dielectric elements with rounded corner cross sections. A comparison with the results obtained by the method of moments and with a commercial simulator is presented for an array of dielectric rods and for a surface-relief diffraction grating.

Index Terms—Spectral methods, mortar-matching, periodic structures, dielectric structures, surface-relief diffraction gratings.

I. INTRODUCTION

PERIODIC structures have been extensively used as models in optics and electromagnetics. For this reason, in recent years many efforts have been made aiming to develop fast and accurate electromagnetic simulators for several problems that involve periodicity. The characterization of reflection gratings has been performed by introducing problem-matched basis functions used to approximate the solution of an integral equation with the method of moments (MoM) [1], and with the mode-matching technique [2]. The frequency response of photonic crystals has been evaluated with a hybrid finite elements method (FEM) exploiting a Floquet mode representation of the electromagnetic field [3] [4]. The two-dimensional scattering of a plane wave from a periodic array of composite dielectric cylinders has been studied with the MoM accelerated by means of a multigrid method [5], or with the aggregate T-matrix method for cylindrical structures [6]. Frequency-selective surfaces have been analyzed by determining numerically the Green's function of a screen perforated by multiply connected apertures [7]. Dielectric frequency-selective surfaces have been analyzed using a vectorial modal method [8]. The boundary integral-resonant mode expansion method (BI-RME) has been

used to study electromagnetic band-gap structures [9]. The finite-difference time-domain method (FDTD) has been used to analyze the guided-wave characteristics of substrate integrated nonradiative dielectric waveguides [10].

The application of spectral methods in the framework of computational electromagnetics is very interesting. These techniques derive from the method of weighted residuals, where the solution of the differential problem is approximated by a linear combination of basis functions defined on a parent domain and mapped to the physical one. The flexibility in the description of the geometry can be enhanced by applying a domain decomposition strategy, giving rise to multi-domain spectral methods, widely applied to computational fluid-dynamics problems [11] [12], and to electromagnetic problems in both frequency and time domains [13], [14], [15]. Then, they have been accelerated and applied to the design of several E-plane and H-plane devices in rectangular waveguide with sharp metallic edges by augmenting the set of basis functions with the asymptotic behavior of the electromagnetic field at metallic corners [16], [17]. Then, a simulator of 2-D dielectric periodic structures has been recently developed starting from [16] and applied to the study of an infinite array of rectangular dielectric rods excited by plane waves with E-plane and H-plane incidence [18], and with skew incidence [19]. This is based on the mortar-element method (MEM), that is a multi-domain spectral method where the continuity conditions between patches are enforced in weak form, according to the mortar-matching technique [12]. The domain decomposition strategy is based on defining patches filled with homogeneous dielectric; by this way, a proper representation of the electromagnetic field in the internal problem can be obtained using a small number of basis functions.

In this paper, the method presented in [19] is further extended to analyze dielectric periodic structures with rounded corners; this feature is used to model the non-idealities caused by manufacturing processes. Subsection II-A describes the decomposition of the original problem into two sub-problems by means of the equivalence theorem: in the first one the field is represented in terms of Floquet modes; the second one consists of a boundary-value differential problem that is solved by means of the MEM, as described in Subsection II-B; this provides the approximate Green's function of the internal problem. In Subsection II-C the two sub-problems are connected through the continuity conditions of the tangential

fields at the access ports. In Section III this numerical scheme is validated by comparison with a MoM code and with the CST Microwave Studio code; then, it is applied to the analysis of a realistic model of a surface-relief diffraction grating.
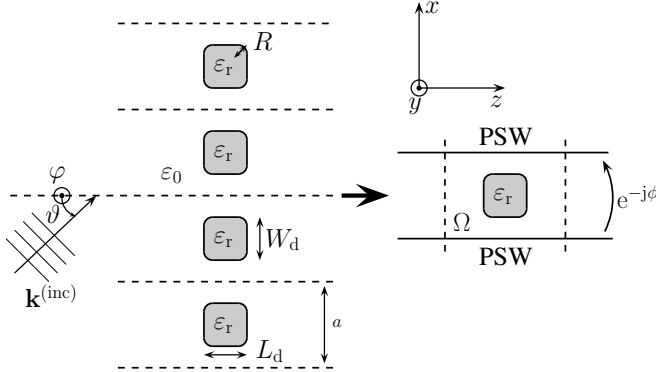

Fig. 1. Left: sketch of the geometry of the structure; right: unit cell. The horizontal solid lines are phase-shift walls (PSW) with phase shift $\phi = k_x^{(\mathrm{inc})} a$; the vertical dashed lines define the access ports; the parameter a is the period; L_d and W_d are the dimensions of the dielectric rod; R is the radius of curvature of the rounded corners.

II. THEORY

The present technique can be applied to the analysis of 2-D periodic structures excited by a plane wave with arbitrary incidence. This is used to compute the generalized scattering matrix in the Floquet modes basis. The geometry sketched in Fig. 1 is used as reference for the description of the formulation; the structure consists of a periodic array of infinitely long dielectric rods with relative permittivity ε_r, surrounded by vacuum. The permittivity is assumed to be complex, to account for possible dielectric losses. The periodicity direction is x and rods are parallel to y. The period of the structure is a, each bar has dimensions L_d and W_d, and the corners are rounded with radius of curvature R. The wavevector of the incident plane wave is

$$\mathbf{k}^{(\mathrm{inc})} = k_0 \left(\sin\vartheta\cos\varphi, \sin\vartheta\sin\varphi, \cos\vartheta\right) =$$
$$= (k_x^{(\mathrm{inc})}, k_y^{(\mathrm{inc})}, k_z^{(\mathrm{inc})}),$$

where k_0 is the free-space wave number. The unit cell consists of a phase-shift wall waveguide with a dielectric obstacle; the pseudo-periodicity boundary conditions for the electric and magnetic fields $\mathbf{E}$ and $\mathbf{H}$ are

$$\begin{cases} \mathbf{E}(z, a) = \mathbf{E}(z, 0)\mathrm{e}^{-\mathrm{j}\phi} \\ \mathbf{H}(z, a) = \mathbf{H}(z, 0)\mathrm{e}^{-\mathrm{j}\phi}, \end{cases}$$

where $\phi = k_x^{(\mathrm{inc})} a$ is the phase shift originated by the incident wave and indicated in Fig. 1.

A. Decomposition of the problem

The original problem is decomposed into two sub-problems: the external one, where the electromagnetic field is non-zero only in the access waveguides, and the internal one, where
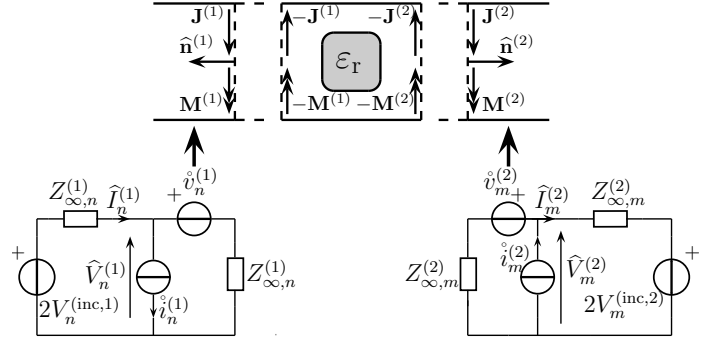

Fig. 2. Top: definition of the two sub-problems; bottom: equivalent multi-modal circuit of the external sub-problem, where only one mode contribution is shown.

the field is non-zero only in the region Ω that contains the dielectric scatterer. In the former, the electromagnetic field is represented by a modal expansion

$$\mathbf{E}_\mathrm{t}^{(k)}(x, y, z) \simeq \sum_{n=1}^{N_\mathrm{m}} V_n^{(k)}(z)\, \mathbf{e}_n(x, y)$$
$$\mathbf{H}_\mathrm{t}^{(k)}(x, y, z) \simeq \sum_{n=1}^{N_\mathrm{m}} I_n^{(k)}(z)\, \mathbf{h}_n(x, y), \tag{1}$$

where N_m is the number of Floquet modes $(\mathbf{e}_n, \mathbf{h}_n)$ used at each port. The equivalence theorem is applied two times for each access port and then two couples of electric and magnetic current densities are introduced on the two sides of the surface $\Sigma_\mathrm{eq}^{(k)}$ located at the k-th access port. Let $\widehat{\mathbf{E}}_\mathrm{t}^{(k)}$, $\widehat{\mathbf{H}}_\mathrm{t}^{(k)}$, ($\widetilde{\mathbf{E}}_\mathrm{t}^{(k)}$, $\widetilde{\mathbf{H}}_\mathrm{t}^{(k)}$) be the transverse electric and magnetic fields on the outer (inner) side of $\Sigma_\mathrm{eq}^{(k)}$. Then,

$$\mathbf{J}^{(k)} = \hat{\mathbf{n}}^{(k)} \times \widehat{\mathbf{H}}_\mathrm{t}^{(k)}, \quad \mathbf{M}^{(k)} = \widehat{\mathbf{E}}_\mathrm{t}^{(k)} \times \hat{\mathbf{n}}^{(k)}, \tag{2}$$

where $\hat{\mathbf{n}}^{(k)}$ is the normal unit vector to $\Sigma_\mathrm{eq}^{(k)}$ directed towards the free-space region; the application of the equivalence theorem is described in the top part of Fig. 2. It is remarked that the equivalent currents $\mathbf{J}^{(k)}$ and $\mathbf{M}^{(k)}$ give rise to $\widehat{\mathbf{E}}_\mathrm{t}^{(k)}$, $\widehat{\mathbf{H}}_\mathrm{t}^{(k)}$ and to a null field inside the region Ω, while $-\mathbf{J}^{(k)}$ and $-\mathbf{M}^{(k)}$ radiate the fields $\widetilde{\mathbf{E}}_\mathrm{t}^{(k)}$ and $\widetilde{\mathbf{H}}_\mathrm{t}^{(k)}$. The current densities are represented by a modal expansion

$$\mathbf{J}^{(k)} \simeq \sum_{n=1}^{N_\mathrm{m}^{(k)}} \mathring{i}_n^{(k)}\mathbf{e}_n, \qquad \mathbf{M}^{(k)} \simeq \sum_{n=1}^{N_\mathrm{m}^{(k)}} \mathring{v}_n^{(k)}\mathbf{h}_n, \tag{3}$$

The position of the access ports is chosen by trading-off the number of the evanescent modes excited by the dielectric obstacle and the number of basis functions that have to be used to represent the solution of the internal problem.

The formulation of the external problem is completed by matching the phase-shift wall waveguides. Then, the equivalent multi-modal circuit shown in the bottom part of Fig. 2 for the n-th mode is derived [20, Chap. 2]; here, the coefficients $\mathring{i}_n^{(k)}$ and $\mathring{v}_n^{(k)}$ have the circuit interpretation of current and voltage sources and $Z_{\infty,n}^{(k)}$ is the modal impedance. This circuit describes, in modal terms, the radiation of the equivalent currents in the external sub-problem.

B. Formulation of the Internal Problem

The boundary-value problem defined in the internal region Ω is derivated from the Maxwell's curl equations, written in cartesian coordinates and in absence of sources. Since the structure is invariant with respect to y, each field component has the same $\mathrm{e}^{-\mathrm{j}k_y y}$ dependence of the incident field. Hence, it is possible to use E_y, H_y as Hertz potentials from which the remaining components are obtained:

$$E_x = -\frac{\mathrm{j}}{k^2 - k_y^2} \left(k_y \frac{\partial E_y}{\partial x} - kZ \frac{\partial H_y}{\partial z} \right)$$

$$E_z = -\frac{\mathrm{j}}{k^2 - k_y^2} \left(k_y \frac{\partial E_y}{\partial z} + kZ \frac{\partial H_y}{\partial x} \right)$$

$$H_x = -\frac{\mathrm{j}}{k^2 - k_y^2} \left(k_y \frac{\partial H_y}{\partial x} + kY \frac{\partial E_y}{\partial z} \right) \tag{4}$$

$$H_z = -\frac{\mathrm{j}}{k^2 - k_y^2} \left(k_y \frac{\partial H_y}{\partial z} - kY \frac{\partial E_y}{\partial x} \right),$$

where $k = k_0$ or $k = k_0\sqrt{\varepsilon_\mathrm{r}}$, depending on the medium, $Z = Z_0$ or $Z = Z_0/\sqrt{\varepsilon_\mathrm{r}}$, where Z_0 is the free-space impedance, and $Y = Z^{-1}$. In the skew incidence case, *i.e.* $\varphi \neq 0$, each field component depends on both E_y and H_y, which are the unknowns of the vector differential problem. If the plane wave is incident in the zx plane (*i.e.* $\varphi = 0$), the problem splits up into independent E-polarization and H-polarization scalar ones, already studied in [18]. The unknowns of the problem are expanded as

$$E_y \simeq \sum_{c=1}^{N_\mathrm{f}} c_c^{(\mathrm{e})} u_c(z, x)$$

$$H_y \simeq \sum_{c=1}^{N_\mathrm{f}} c_c^{(\mathrm{h})} u_c(z, x), \tag{5}$$

where the expansion functions $u_c(z, x)$ belong to the function space V of continuous functions with integrable derivatives satisfying the pseudo-periodicity condition

$$u_c(z, a) = u_c(z, 0)\mathrm{e}^{-\mathrm{j}\phi} \quad z \in [0, L] \quad \forall c = 1...N_\mathrm{f}. \tag{6}$$

The synthesis of these basis functions is performed according to the mortar-element method, which consists in decomposing the region Ω into patches that are mapped to a square parent domain by means of blending mappings. The Gordon-Hall formula is used to obtain the mappings from the parent domain to a generic quadrilateral with either rounded or straight edges [12, Sect. 8.8.4]; this is a generalization of the bilinear mapping used in [18], [19]. A set of local basis functions is defined on the parent domain for each patch, and then these functions are specialized to satisfy the essential boundary conditions, that involve the continuity between adjacent patches and the pseudo-periodicity. The procedure used to synthesize the basis functions is extensively discussed in [16].

Equations (4) are obtained from the x and z components of the curl Maxwell's equations. The y components are cast in weak form by projecting them onto a set of test functions $v_r = u_r$ chosen according to the Galerkin version of the method of weighted residuals

$$\left\langle \frac{\partial E_x}{\partial z} - \frac{\partial E_z}{\partial x}, v_r \right\rangle = -\mathrm{j}kZ \left\langle H_y, v_r \right\rangle$$

$$\left\langle \frac{\partial H_x}{\partial z} - \frac{\partial H_z}{\partial x}, v_r \right\rangle = \left\langle \mathrm{j}kY E_y, v_r \right\rangle.$$

Then, integration by parts by means of Stokes theorem is performed and the following equations are obtained:

$$(\mathrm{LHS})_r^{(\mathrm{e})} = (\mathrm{RHS})_r^{(\mathrm{e})} \qquad \forall r = 1...N_\mathrm{f} \tag{7}$$

$$(\mathrm{LHS})_r^{(\mathrm{h})} = (\mathrm{RHS})_r^{(\mathrm{h})} \qquad \forall r = 1...N_\mathrm{f}, \tag{8}$$

where

$$(\mathrm{LHS})_r^{(\mathrm{e})} = \mathrm{j} \iint_\Omega kY E_y v_r^* \mathrm{d}x\,\mathrm{d}z +$$

$$+ \iint_\Omega \left[H_x \frac{\partial v_r^*}{\partial z} - H_z \frac{\partial v_r^*}{\partial x} \right] \mathrm{d}x\,\mathrm{d}z \tag{9}$$

$$(\mathrm{RHS})_r^{(\mathrm{e})} = \oint_\gamma (\mathbf{H}_\mathrm{t}^{(y)} v_r^*) \cdot \mathrm{d}\mathbf{s} \tag{10}$$

$$(\mathrm{LHS})_r^{(\mathrm{h})} = -\mathrm{j}kZ \iint_\Omega H_y v_r^* \mathrm{d}x\,\mathrm{d}z +$$

$$+ \iint_\Omega \left[E_x \frac{\partial v_r^*}{\partial z} - E_z \frac{\partial v_r^*}{\partial x} \right] \mathrm{d}x\,\mathrm{d}z \tag{11}$$

$$(\mathrm{RHS})_r^{(\mathrm{h})} = \oint_\gamma (\mathbf{E}_\mathrm{t}^{(y)} v_r^*) \cdot \mathrm{d}\mathbf{s}, \tag{12}$$

and $\gamma = \gamma_\mathrm{PSW} \cup \gamma_\mathrm{wg}^{(1)} \cup \gamma_\mathrm{wg}^{(2)}$ is the boundary of Ω, $\mathbf{E}_\mathrm{t}^{(y)}$ and $\mathbf{H}_\mathrm{t}^{(y)}$ are the electric and magnetic fields transverse to y. The top and bottom contributions (on γ_PSW) to the RHS integrals are set equal to zero to enforce the pseudo-periodicity of E_x, E_z, H_x, H_z as natural boundary conditions [21, Chap. 3]. Then, the two remaining contributions (on $\gamma_\mathrm{wg}^{(k)}$) are used to account for the effect of the equivalent currents as non-homogeneous boundary conditions. By observing that $\mathbf{E}_\mathrm{t}^{(y)} \cdot \mathrm{d}\mathbf{s} = \widetilde{\mathbf{E}}_\mathrm{t}^{(k)} \cdot \mathrm{d}\mathbf{s}$ and $\mathbf{H}_\mathrm{t}^{(y)} \cdot \mathrm{d}\mathbf{s} = \widetilde{\mathbf{H}}_\mathrm{t}^{(k)} \cdot \mathrm{d}\mathbf{s}$,

$$(\mathrm{RHS})_r^{(\mathrm{e})} = b_r^{(\mathrm{e},1)} + b_r^{(\mathrm{e},2)}$$

$$(\mathrm{RHS})_r^{(\mathrm{h})} = b_r^{(\mathrm{h},1)} + b_r^{(\mathrm{h},2)}, \tag{13}$$

where, according to (2) and enforcing the field continuity:

$$b_r^{(\mathrm{e},k)} = \int_{\gamma_\mathrm{wg}^{(k)}} (\widetilde{\mathbf{H}}_\mathrm{t}^{(k)} v_r^*) \cdot \mathrm{d}\mathbf{s} =$$

$$\int_{\gamma_\mathrm{wg}^{(k)}} (\mathbf{J}^{(k)} \times \hat{\mathbf{n}}^{(k)} v_r^{(\mathrm{e})*}) \cdot \mathrm{d}\mathbf{s}$$

$$b_r^{(\mathrm{h},k)} = \int_{\gamma_\mathrm{wg}^{(k)}} (\widetilde{\mathbf{E}}_\mathrm{t}^{(k)} v_r^*) \cdot \mathrm{d}\mathbf{s} = \tag{14}$$

$$\int_{\gamma_\mathrm{wg}^{(k)}} (\hat{\mathbf{n}}^{(k)} \times \mathbf{M}^{(k)} v_r^{(\mathrm{h})*}) \cdot \mathrm{d}\mathbf{s}.$$

By substituting (4) and (5) in (9) and (11) the following system of matrix equations is obtained:

$$\begin{cases} \mathbf{A}^{(\mathrm{e},\mathrm{e})} \mathbf{c}^{(\mathrm{e})} + \mathbf{A}^{(\mathrm{e},\mathrm{h})} \mathbf{c}^{(\mathrm{h})} = \mathbf{b}^{(\mathrm{e},2)} + \mathbf{b}^{(\mathrm{e},1)} \\ \mathbf{A}^{(\mathrm{h},\mathrm{e})} \mathbf{c}^{(\mathrm{e})} + \mathbf{A}^{(\mathrm{h},\mathrm{h})} \mathbf{c}^{(\mathrm{h})} = \mathbf{b}^{(\mathrm{h},2)} + \mathbf{b}^{(\mathrm{h},1)}, \end{cases} \tag{15}$$

being $\mathbf{c}^{(\mathrm{e})}$ and $\mathbf{c}^{(\mathrm{h})}$ the vectors obtained collecting the expansion coefficients defined in (5). The vectors $\mathbf{b}^{(\mathrm{e},k)}$ and $\mathbf{b}^{(\mathrm{h},k)}$

contain the line integrals defined in (13) and are expressed in terms of the source coefficients $\mathbf{i}^{(k)}$ and $\mathbf{v}^{(k)}$ by using (3),

$$\begin{aligned} \mathbf{b}^{(\mathrm{e},k)} &= \mathbf{B}^{(\mathrm{e},k)}\,\mathring{\mathbf{i}}^{(k)} \\ \mathbf{b}^{(\mathrm{h},k)} &= \mathbf{B}^{(\mathrm{h},k)}\,\mathring{\mathbf{v}}^{(k)}. \end{aligned} \tag{16}$$

This leads to the definition of the matrix equation

$$\mathbf{A}\,\mathbf{c} = \mathbf{B}\,\mathbf{x},$$

where

$$\mathbf{c} = \begin{bmatrix} \mathbf{c}^{(\mathrm{e})} \\ \mathbf{c}^{(\mathrm{h})} \end{bmatrix}, \qquad \mathbf{x} = \begin{bmatrix} \mathring{\mathbf{i}}^{(1)} \\ \mathring{\mathbf{v}}^{(1)} \\ \mathring{\mathbf{i}}^{(2)} \\ \mathring{\mathbf{v}}^{(2)} \end{bmatrix}. \tag{17}$$

By inverting this expression it is obtained

$$\mathbf{c} = \mathbf{G}\,\mathbf{x}. \tag{18}$$

This equation provides a relationship between the current densities defined at each access port and the field that they radiate in the region Ω; for this reason, the matrix $\mathbf{G} = \mathbf{A}^{-1}\mathbf{B}$ can be interpreted a representation of the Green's function of the internal problem.

C. Continuity equations at the access ports

The formulation of the method is completed by coupling the internal and external sub-problems through the continuity conditions of the transverse fields at the access ports. The transverse field continuity at the k-th port is enforced by projection on the mode functions

$$\begin{cases} \langle \widetilde{\mathbf{E}}_{\mathrm{t}}^{(k)}, \mathbf{e}_q^{(k)} \rangle = \langle \widehat{\mathbf{E}}_{\mathrm{t}}^{(k)}, \mathbf{e}_q^{(k)} \rangle & \forall q = 1...N_{\mathrm{m}} \\ \langle \widetilde{\mathbf{H}}_{\mathrm{t}}^{(k)}, \mathbf{h}_q^{(k)} \rangle = \langle \widehat{\mathbf{H}}_{\mathrm{t}}^{(k)}, \mathbf{h}_q^{(k)} \rangle & \forall q = 1...N_{\mathrm{m}}. \end{cases} \tag{19}$$

The fields $\widehat{\mathbf{E}}_{\mathrm{t}}^{(k)}$, $\widehat{\mathbf{H}}_{\mathrm{t}}^{(k)}$ are represented in terms of Floquet modes, while $\widetilde{\mathbf{E}}_{\mathrm{t}}^{(k)}$ and $\widetilde{\mathbf{H}}_{\mathrm{t}}^{(k)}$ using the MEM basis functions restricted to the k-th port. By recalling (1), this equation is written in matrix form

$$\begin{cases} \mathbf{T}_k^{(\mathrm{e,e})}\mathbf{c}^{(\mathrm{e})} + \mathbf{T}_k^{(\mathrm{e,h})}\mathbf{c}^{(\mathrm{h})} = \widehat{\mathbf{V}}^{(k)} \\ \mathbf{T}_k^{(\mathrm{h,e})}\mathbf{c}^{(\mathrm{e})} + \mathbf{T}_k^{(\mathrm{h,h})}\mathbf{c}^{(\mathrm{h})} = \widehat{\mathbf{I}}^{(k)} \end{cases}, \tag{20}$$

where the matrices $\mathbf{T}_k^{(\cdot,\cdot)}$ contain the projections of the MEM basis functions on the k-th waveguide modes. By expressing the right-hand sides of the previous equations in terms of the generators and the incident fields (see Appendix A), the following matrix equation is obtained,

$$\mathbf{T}\,\mathbf{c} = \mathbf{D}\,\mathbf{x} + \mathbf{K}\,\mathbf{V}^{(\mathrm{inc})}. \tag{21}$$

Then, by substituting (18) in (21),

$$\mathbf{x} = [\mathbf{T}\,\mathbf{G} - \mathbf{D}]^{-1}\,\mathbf{K}\,\mathbf{V}^{(\mathrm{inc})}. \tag{22}$$

The expressions of all the matrix elements are reported in Appendix A. Once $\mathbf{x}$ is known, it is possible to compute the
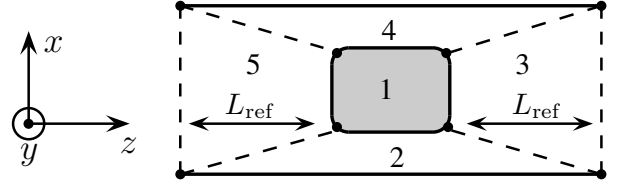

Fig. 3. Domain decomposition approach applied to the structure of Fig. 1; the dashed lines and the numbers identify the patches and the dots identify their vertexes. The distance from the access ports if L_{ref}. The patch 1 is filled with dielectric $\varepsilon_{\mathrm{r}} = n^2$.

generalized scattering matrix $\mathbf{S}$ of the structure and to use (18) to evaluate the electromagnetic field in the device, as reported in Appendix B.

III. RESULTS

In this section the mortar-element method is validated through a comparison with results obtained with a MoM code and with the CST Microwave Studio frequency domain solver (CST-MS). In all the following examples, the dielectric losses are neglected. The integrals involved in the evaluation of the matrix elements are calculated with a Gauss-Legendre quadrature rule with $N_{\mathrm{quad}} = 32$ nodes.

A. Array of dielectric rods

The first benchmark case is the array of dielectric rods shown in Fig. 1. The domain decomposition approach applied to this structure is described in Fig. 3, where five patches have been adopted. It is convenient to choose the vertexes of the patches in such a way that the angles between their edges are as close to $90°$ as possible, to have regular mappings to the parent domain; in this case, the best possibility is to choose the center of the arcs. It has to be remarked that, at the interfaces between different dielectrics, some field derivatives are discontinuous; for this reason, it is convenient to divide the domain Ω in patches where the dielectric is homogeneous, to avoid Gibbs phenomena.

The geometry of the structure is defined by: $a = 100$ μm, $L_{\mathrm{d}} = 40$ μm, $W_{\mathrm{d}} = 30$ μm. The access ports are located $L_{\mathrm{ref}} = 55$ μm from each vertical dielectric interface, the refractive index in the patch 1 is $n = 2.21$.

In Figs. 4 and 5 the TE_0-TE_0 reflection coefficient is reported versus frequency and incidence angle ϑ. In both analyses, $N_{\mathrm{m}} = 8$ modes have been used to represent the electromagnetic field at each access port and $N_{\mathrm{f}} = 84$ entire-domain basis functions (generated by means of fifth-degree polynomials) are used to represent E_y and H_y. In Fig. 4, $\vartheta = 55°$, $\varphi = 20°$; in Fig. 5, $f = 1.2$ THz. The reference solution has been obtained by an in-house MoM code where $N_{\mathrm{m,MoM}} = 50$ modes are used to approximate the Green's function [22], [23]. This choice ensures the convergence of the scattering parameter. Good agreement between the curves can be observed even if in the available MoM code the corners are assumed to be sharp, whereas in the MEM code they are rounded with $R = L_{\mathrm{d}}/40$.
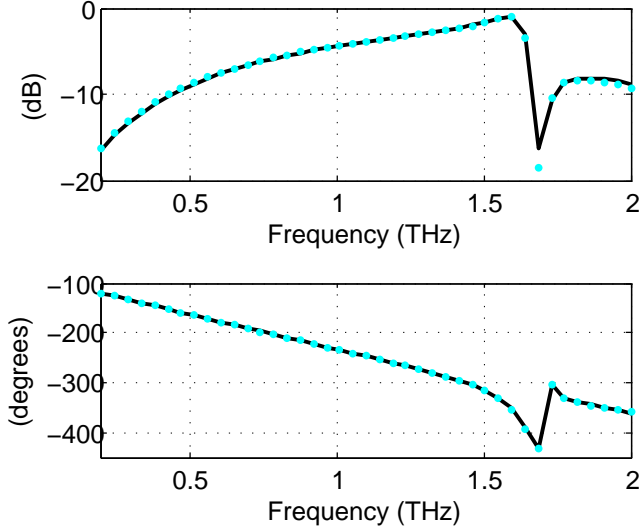
Fig. 4. Magnitude and phase of the TE_0 mode reflection coefficient of the array of dielectric rods of Fig. 3, with $R = L_d/40$. The solid and dotted curves refer to the MEM and with MoM simulations.
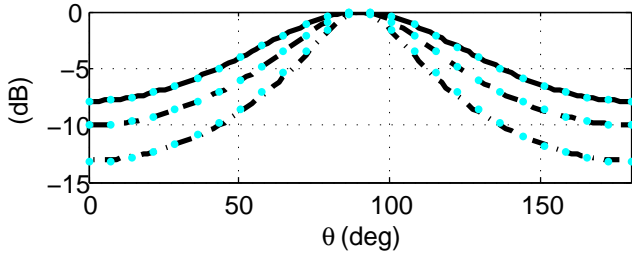

Fig. 5. Magnitude of the TE_0-TE_0 mode reflection coefficient for the array of dielectric rods of Fig. 3, with $R = L_d/40$, $f = 1.2$ THz. The solid, dashed and dash-dotted lines refer to results obtained with $\varphi = 20°, 40°, 60°$ with the MEM technique. The brighter, dotted lines refer to the results obtained with MoM.

Fig. 6. Magnitude and phase of the TE_0-TE_0 mode reflection coefficient for the array of dielectric rods of Fig. 3, with $R = L_d/4$. The solid and dotted curves refer to results obtained with the MEM technique and with CST-MS, respectively.

Fig. 7. Magnitude of the TE_0-TE_0 mode reflection coefficient for the array of dielectric rods of Fig. 3. The curves from right to left refer to $R = L_d/3, R = L_d/4, R = L_d/6, R = L_d/9, R = L_d/40$.
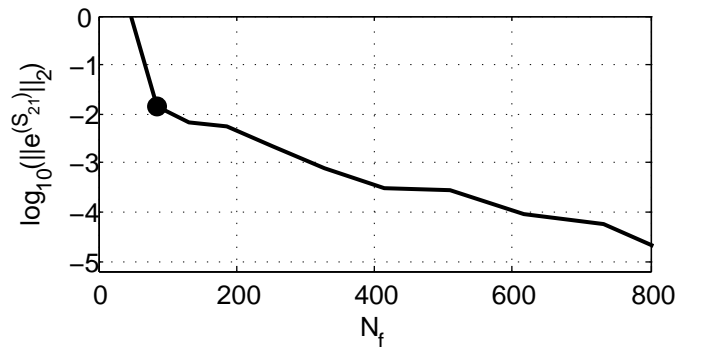
Fig. 8. Convergence analysis of the MEM applied to the array of dielectric rods of Fig. 3. The curves report the 2-norm relative error $\left\|e^{(S_{21})}\right\|_2$ in the transmission coefficient versus the number of functions used to represent each unknown of the differential problem. The dot refers to the simulations of Fig. 6.

In Fig. 6 a comparison between the TE_0-TE_0 reflection coefficient simulated with the MEM code and with CST-MS is shown for the same structure with radii of curvature of the corners changed to $R = L_d/4$, for a plane wave with incidence angles $\vartheta = 55°$, $\varphi = 20°$; a remarkable agreement is achieved also in this case.

In Fig. 7 the TE_0-TE_0 reflection coefficient obtained with the MEM for several values of the curvature radius R is reported. The main effect of the R variation is a small shift of the reflection zero.

Figure 8 shows the convergence study of the 2-norm relative error of the TE_0-TE_0 transmission coefficient versus the number of functions N_f for $R = L_d/4$. The dot refers to the MEM simulation shown in Fig. 6 for which an accuracy better than 1% is achieved. It is shown that the scheme exhibits the typical exponentially-convergent behavior of spectral methods.

B. Surface-relief diffraction grating

As a second test case the MEM has been used to analyze a surface-relief diffraction grating, where the rounded corners
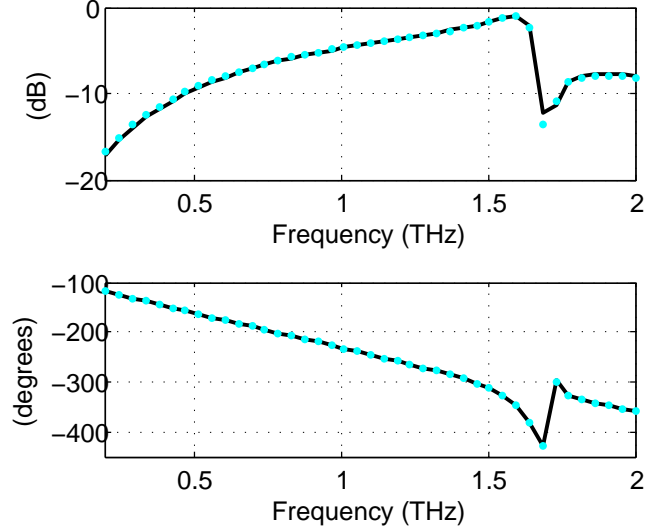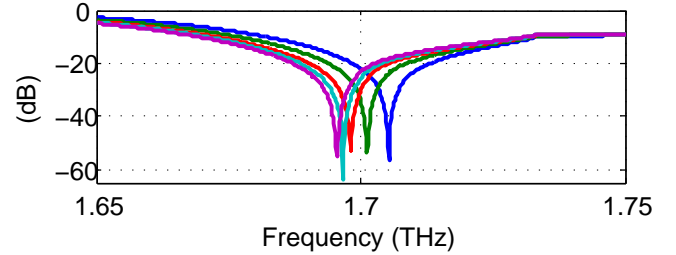
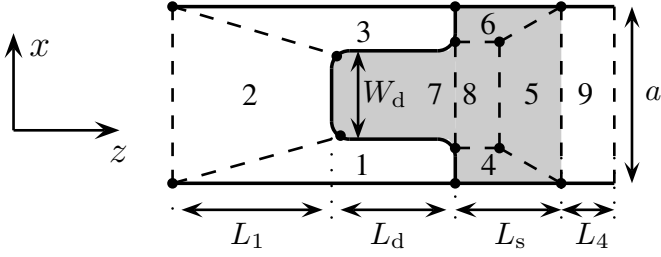Fig. 9. Domain decomposition approach applied to the realistic model of a surface-relief diffraction grating. The patches $4 \div 8$ are filled with dielectric $\varepsilon_{\mathrm{r}} = n^2$, the remaining ones with vacuum; the dots identify the vertexes of the patches; all the corners are rounded, with radius of curvature R.
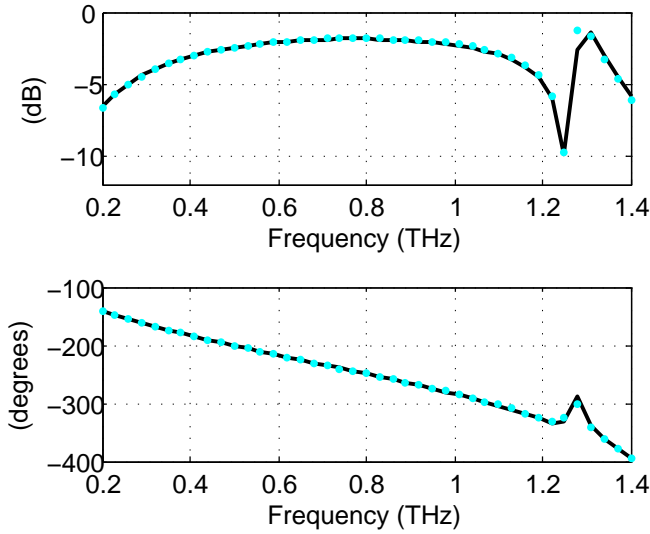

Fig. 10. Magnitude and phase of the TE_0-TE_0 reflection coefficient for the surface-relief diffraction grating of Fig. 9, with $R = L_{\mathrm{d}}/4$. The solid and dotted curves refer to results obtained with the MEM technique and with CST-MS, respectively.

Fig. 11. Magnitude and phase of the TM_0-TM_0 reflection coefficient for the surface-relief diffraction grating of Fig. 9, with $R = L_{\mathrm{d}}/4$. The solid and dotted curves refer to results obtained with the MEM technique and with CST-MS, respectively.
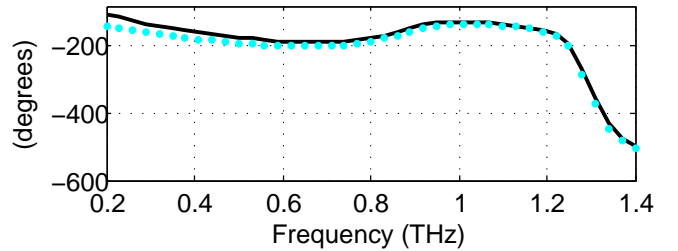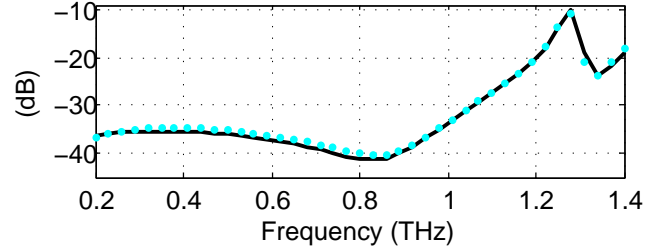
Fig. 12. Magnitude and phase of the TM_0-TE_0 (TE_0 incident) reflection coefficient for the surface-relief diffraction grating of Fig. 9, with $R = L_{\mathrm{d}}/4$. The solid and dotted curves refer to results obtained with the MEM technique and with CST-MS.

take into account the non-idealities associated to the manufacturing process. A detailed review of the fabrication issues occurring in the case of optical applications can be found in [24, Sect. 1.6]. The geometry of this structure and its patching are reported in Fig. 9. The period is $a = 100$ μm, the dielectric tooth dimensions are $L_{\mathrm{d}} = 35$ μm and $W_{\mathrm{d}} = 40$ μm, the distance of the left port from the dielecric is $L_1 = 50$ μm, the height of the dielectric substrate is $L_{\mathrm{s}} = 25$ μm, the distance of the right port from the substrate is $L_2 = 25$ μm, $R = L_{\mathrm{d}}/4$, the refractive index of the dielectric is $n = 2.21$, the incidence direction is $\vartheta = 55°$, $\varphi = 20°$.

In Figs. 10, 11 and 12 the comparisons of the TE_0-TE_0, TM_0-TM_0 and TM_0-TE_0, reflection coefficients simulated with the MEM code and with CST-MS are reported. $N_{\mathrm{f}} = 84$ entire domain basis functions (generated by polynomials of degree 4) and $N_{\mathrm{m}} = 4$ modes have been used in the MEM simulations. A remarkable agreement has been achieved also for very low levels of reflection coefficient.
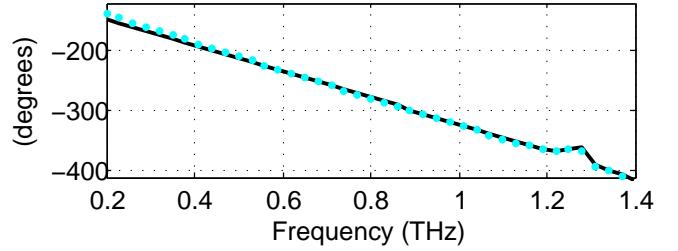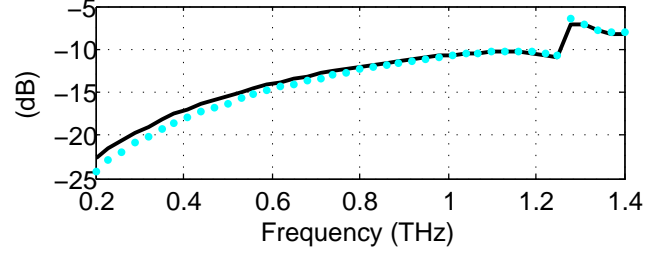
IV. CONCLUSION

The formulation of the plane wave scattering problem from a dielectric periodic structure has been presented; this is based on decomposing the problem into an external sub-problem where the field is represented using Floquet modes, and a sub-problem where the field is found as the solution of a differential problem with pseudo-periodicity boundary conditions. This has been solved by means of the mortar-element method. The results of this technique have been compared to reference solutions obtained with a MoM code and with a commercial code. This procedure validated the numerical method.

APPENDIX A
EXPRESSIONS OF THE MATRIX ELEMENTS

In this appendix the expressions of the elements of the matrices introduced in Section II are explicitly reported. The matrix $\mathbf{A}$ is defined as

$$\mathbf{A} = \begin{bmatrix} \mathbf{A}^{(\mathrm{e,e})} & \mathbf{A}^{(\mathrm{e,h})} \\ \mathbf{A}^{(\mathrm{h,e})} & \mathbf{A}^{(\mathrm{h,h})} \end{bmatrix},$$

where:

$$\mathbf{A}^{(\mathrm{e,e})} = \frac{jkY}{k^2 - k_y^2} \left[(k^2 - k_y^2)\mathbf{M} - \mathbf{N} \right]$$

$$\mathbf{A}^{(\mathrm{e,h})} = \frac{jk_y}{k^2 - k_y^2} \mathbf{L}$$

$$\mathbf{A}^{(\mathrm{h,e})} = \frac{jk_y}{k^2 - k_y^2} \mathbf{L}$$

$$\mathbf{A}^{(\mathrm{h,h})} = -\frac{jkZ}{k^2 - k_y^2} \left[(k^2 - k_y^2)\mathbf{M} - \mathbf{N} \right]$$

and:

$$(\mathbf{M})_{rc} = \iint_\Omega u_c v_r^* \, \mathrm{d}z \, \mathrm{d}x$$

$$(\mathbf{N})_{rc} = \iint_\Omega \left[\frac{\partial u_c}{\partial z} \frac{\partial v_r^*}{\partial z} + \frac{\partial u_c}{\partial x} \frac{\partial v_r^*}{\partial x} \right] \mathrm{d}z \, \mathrm{d}x$$

$$(\mathbf{L})_{rc} = \iint_\Omega \left[\frac{\partial u_c}{\partial z} \frac{\partial v_r^*}{\partial x} - \frac{\partial u_c}{\partial x} \frac{\partial v_r^*}{\partial z} \right] \mathrm{d}z \, \mathrm{d}x.$$

The matrix $\mathbf{B}$ is defined as

$$\mathbf{B} = \begin{bmatrix} -\mathbf{B}^{(\mathrm{e},1)} & \mathbf{0} & \mathbf{B}^{(\mathrm{e},2)} & \mathbf{0} \\ \mathbf{0} & -\mathbf{B}^{(\mathrm{h},1)} & \mathbf{0} & \mathbf{B}^{(\mathrm{h},2)} \end{bmatrix},$$

where, for the k-th port:

$$(\mathbf{B}^{(\mathrm{e},k)})_{rn} = \int_0^a h_{x,n} v_r^* \Big|_{\Sigma_{\mathrm{eq}}^{(k)}} \, \mathrm{d}x$$

$$(\mathbf{B}^{(\mathrm{h},k)})_{rn} = \int_0^a e_{x,n} v_r^* \Big|_{\Sigma_{\mathrm{eq}}^{(k)}} \, \mathrm{d}x.$$

As for the system (20) associated to the continuity conditions at the waveguide ports, the matrix $\mathbf{T}$ containing the projections of the MEM basis functions on the Floquet modes is

$$\mathbf{T} = \begin{bmatrix} \mathbf{T}_1^{(\mathrm{e,e})} & \mathbf{T}_1^{(\mathrm{e,h})} \\ \mathbf{T}_1^{(\mathrm{h,e})} & \mathbf{T}_1^{(\mathrm{h,h})} \\ \mathbf{T}_2^{(\mathrm{e,e})} & \mathbf{T}_2^{(\mathrm{e,h})} \\ \mathbf{T}_2^{(\mathrm{h,e})} & \mathbf{T}_2^{(\mathrm{h,h})} \end{bmatrix},$$

where:

$$(\mathbf{T}_k^{(\mathrm{e,e})})_{rc} = \int_0^a \left[u_c e_{y,r}^* - \frac{jk_y}{k^2 - k_y^2} \frac{\partial u_c}{\partial x} e_{x,r}^* \right] \Bigg|_{\Sigma_{\mathrm{eq}}^{(k)}} \, \mathrm{d}x$$

$$(\mathbf{T}_k^{(\mathrm{e,h})})_{rc} = \int_0^a \frac{jkZ}{k^2 - k_y^2} \frac{\partial u_c}{\partial z} e_{x,r}^* \Bigg|_{\Sigma_{\mathrm{eq}}^{(k)}} \, \mathrm{d}x$$

$$(\mathbf{T}_k^{(\mathrm{h,e})})_{rc} = - \int_0^a \frac{jkY}{k^2 - k_y^2} \frac{\partial u_c}{\partial z} h_{x,r}^* \Bigg|_{\Sigma_{\mathrm{eq}}^{(k)}} \, \mathrm{d}x$$

$$(\mathbf{T}_k^{(\mathrm{h,h})})_{rc} = \int_0^a \left[u_c h_{y,r}^* - \frac{jk_y}{k^2 - k_y^2} \frac{\partial u_c}{\partial x} h_{x,r}^* \right] \Bigg|_{\Sigma_{\mathrm{eq}}^{(k)}} \, \mathrm{d}x.$$

For the circuit shown in Fig. 2, the voltage and current on the transmission lines are found as:

$$\begin{cases} \widehat{\mathbf{V}}^{(1)} = \mathbf{V}^{(1,\mathrm{inc})} - \frac{1}{2}\mathbf{Z}_\infty^{(1)} \cdot \mathring{\mathbf{i}}^{(1)} + \frac{1}{2}\mathring{\mathbf{v}}^{(1)} \\ \widehat{\mathbf{I}}^{(1)} = \mathbf{Y}_\infty^{(1)} \cdot \mathbf{V}^{(1,\mathrm{inc})} + \frac{1}{2}\mathring{\mathbf{i}}^{(1)} - \frac{1}{2}\mathbf{Y}_\infty^{(1)} \cdot \mathring{\mathbf{v}}^{(1)} \\ \widehat{\mathbf{V}}^{(2)} = \mathbf{V}^{(2,\mathrm{inc})} + \frac{1}{2}\mathbf{Z}_\infty^{(2)} \cdot \mathring{\mathbf{i}}^{(2)} + \frac{1}{2}\mathring{\mathbf{v}}^{(2)} \\ \widehat{\mathbf{I}}^{(2)} = -\mathbf{Y}_\infty^{(2)} \cdot \mathbf{V}^{(2,\mathrm{inc})} + \frac{1}{2}\mathring{\mathbf{i}}^{(2)} + \frac{1}{2}\mathbf{Y}_\infty^{(2)} \cdot \mathring{\mathbf{v}}^{(2)}, \end{cases} \quad (23)$$

where $\mathbf{Z}_\infty^{(k)}$ and $\mathbf{Y}_\infty^{(k)}$ are the diagonal matrices containing the modal characteristic impedances and admittances in the k-th waveguide. Then the matrices $\mathbf{D}$ and $\mathbf{K}$ are defined by grouping the right-hand side of (20). The matrix $\mathbf{D}$ is

$$\mathbf{D} = \begin{bmatrix} -\frac{1}{2}\mathbf{Z}_\infty^{(1)} & \frac{1}{2}\mathbf{I} & \mathbf{0} & \mathbf{0} \\ \frac{1}{2}\mathbf{I} & -\frac{1}{2}\mathbf{Y}_\infty^{(1)} & \mathbf{0} & \mathbf{0} \\ \mathbf{0} & \mathbf{0} & \frac{1}{2}\mathbf{Z}_\infty^{(2)} & \frac{1}{2}\mathbf{I} \\ \mathbf{0} & \mathbf{0} & \frac{1}{2}\mathbf{I} & \frac{1}{2}\mathbf{Y}_\infty^{(2)} \end{bmatrix},$$

where $\mathbf{I}$ is the identity matrix and $\mathbf{0}$ is a matrix filled with zeros. Similarly, the matrix $\mathbf{K}$ is

$$\mathbf{K} = \begin{bmatrix} \mathbf{I} & \mathbf{0} \\ \mathbf{Y}_\infty & \mathbf{0} \\ \mathbf{0} & \mathbf{I} \\ \mathbf{0} & -\mathbf{Y}_\infty^{(2)} \end{bmatrix}.$$

APPENDIX B
COMPUTATION OF THE GENERALIZED SCATTERING MATRIX

In this appendix the computation of the GSM of the device is described. The modal voltage in the k-th waveguide can be written as the sum of the incident and the scattered waves

$$\widehat{\mathbf{V}}^{(k)} = \widehat{\mathbf{V}}^{(\mathrm{inc},k)} + \widehat{\mathbf{V}}^{(\mathrm{scat},k)} = (\mathbf{Z}_\infty^{(k)})^{\frac{1}{2}}(\mathbf{a}^{(k)} + \mathbf{b}^{(k)}).$$

By combining this representation with (23), the scattered wave amplitudes are written as

$$\begin{cases} \mathbf{b}^{(1)} = -\frac{1}{2}(\mathbf{Z}_{\infty}^{(1)})^{\frac{1}{2}}\mathring{\mathbf{i}}^{(1)} + \frac{1}{2}(\mathbf{Y}_{\infty}^{(1)})^{\frac{1}{2}}\mathring{\mathbf{v}}^{(1)} \\ \mathbf{b}^{(2)} = +\frac{1}{2}(\mathbf{Z}_{\infty}^{(2)})^{\frac{1}{2}}\mathring{\mathbf{i}}^{(2)} + \frac{1}{2}(\mathbf{Y}_{\infty}^{(2)})^{\frac{1}{2}}\mathring{\mathbf{v}}^{(2)}, \end{cases} \quad (24)$$

or, more compactly,

$$\mathbf{b} = \frac{1}{2}\mathbf{P}\,\mathbf{x},$$

where:

$$\mathbf{P} = \begin{bmatrix} -(\mathbf{Z}_{\infty}^{(1)})^{\frac{1}{2}} & (\mathbf{Y}_{\infty}^{(1)})^{\frac{1}{2}} & \mathbf{0} & \mathbf{0} \\ \mathbf{0} & \mathbf{0} & (\mathbf{Z}_{\infty}^{(2)})^{\frac{1}{2}} & (\mathbf{Y}_{\infty}^{(2)})^{\frac{1}{2}} \end{bmatrix}$$

$$\mathbf{b} = \begin{bmatrix} \mathbf{b}^{(1)} \\ \mathbf{b}^{(2)} \end{bmatrix}.$$

Then, according to (22), (24) becomes

$$\mathbf{b} = \frac{1}{2}\mathbf{P}\left[\mathbf{T}\,\mathbf{G} - \mathbf{D}\right]^{-1}\mathbf{K}\,\mathbf{Q}\,\mathbf{a}$$

because:

$$\mathbf{V}^{(\text{inc})} = \begin{bmatrix} \mathbf{V}^{(\text{inc},1)} \\ \mathbf{V}^{(\text{inc},2)} \end{bmatrix} = \mathbf{Q}\,\mathbf{a}$$

and

$$\mathbf{Q} = \begin{bmatrix} (\mathbf{Z}_{\infty}^{(1)})^{\frac{1}{2}} & \mathbf{0} \\ \mathbf{0} & (\mathbf{Z}_{\infty}^{(2)})^{\frac{1}{2}} \end{bmatrix}, \quad \mathbf{a} = \begin{bmatrix} \mathbf{a}^{(1)} \\ \mathbf{a}^{(2)} \end{bmatrix},$$

from which, the expression of the GSM is obtained

$$\mathbf{S} = \frac{1}{2}\mathbf{P}\left[\mathbf{T}\,\mathbf{G} - \mathbf{D}\right]^{-1}\mathbf{K}\,\mathbf{Q}.$$

REFERENCES

[1] C. K. Aanandan, P. Debernardi, R. Orta, R. Tascone, and D. Trinchero, "Problem-matched basis functions for moment method analysis - an application to reflection gratings," *IEEE Trans. Antennas Propag.,* vol. 48, pp. 35-40, Jan. 2000.

[2] A. Coves, B. Gimeno, A. A. San Blas, A. Vidal, V. E. Boria, and M. V. Andrés, "Three-dimensional scattering of dielectric gratings under plane-wave excitation," *IEEE Antennas Wireless Propag. Lett.*, vol. 2, no. 1, pp. 215-218, 2003.

[3] G. Pelosi, A. Cocchi, and A. Monorchio, "A hybrid FEM-based procedure for the scattering from photonic crystals illuminated by a gaussian beam," *IEEE Trans. Antennas Propag.,* vol. 48, no. 6, pp. 973-980, June 2000.

[4] G. Pelosi, A. Freni, and R. Coccioli, "Hybrid technique for analysing scattering from periodic structures," *IEE Proceedings H on Microwaves, Antennas and Propagation,* vol. 140, no. 2, pp. 65-70, Apr. 1993.

[5] M. Yokota and M. Sesay, "Two-dimensional scattering of a plane wave from a periodic array of dielectric cylinders with arbitrary shape," *J. Opt. Soc. Am.,* vol. 25, no. 7, pp. 1691-1696, July 2008.

[6] H. Toyama and K. Yasumoto, "Electromagnetic scattering from periodic arrays of composite circular cylinder with internal cylindrical scatterers," *Progress In Electromagnetics Research (PIER),* vol. 52, pp. 321-333, 2005.

[7] R. Orta, P. Savi, and R. Tascone, "Numerical Green's function technique for the analysis of screens perforated by multiply connected apertures," *IEEE Trans. Antennas Propag.,* vol. 44, pp. 765-776, June 1996.

[8] A. Coves, B. Gimeno, J. Gil, M. V. Andrés, A. A. S. Blas, and V. E. Boria, "Full-wave analysis of dielectric frequency-selective surfaces using a vectorial modal method," *IEEE Trans. Antennas Propag.,* vol. 52, no. 8, pp. 2091-2099, Aug. 2004.

[9] M. Bozzi, S. Germani, L. Minelli, L. Perregrini, and P. de Maagt, "Efficient calculation of the dispersion diagram of planar electromagnetic band-gap structures by the MoM/BI-RME method," *IEEE Trans. Antennas Propag.,* vol. 53, no. 1, pp. 29-35, Jan. 2005.

[10] F. Xu, K. Wu, and W. Hong, "Finite-difference time-domain modeling of periodic guided-wave structures and its application to the analysis of substrate integrated nonradiative dielectric waveguide," *IEEE Trans. Microw. Theory Techn.,* vol. 55, no. 12, pp. 2502-2511, Dec 2007.

[11] C. Canuto, M. Y. Hussaini, A. Quarteroni, and T. A. Zang, "Spectral methods: fundamentals in single domains," Berlin, Germany: Springer-Verlag, 2006.

[12] C. Canuto, M. Y. Hussaini, A. Quarteroni, and T. A. Zang, "Spectral methods: evolution to complex geometries and applications to fluid dynamics," Berlin, Germany: Springer-Verlag, 2007.

[13] J. H. Lee, T. Xiao, and Q. H. Liu, "A 3-D spectral-element method using mixed-order curl conforming vector basis functions for electromagnetics fields," *IEEE Trans. Microw. Theory Techn.,* vol. 54, no. 1, pp. 437-444, Jan. 2006.

[14] Y. Liu, J. H. Lee, T. Xiao, and Q. H. Liu, "A spectral-element time-domain solution of Maxwell's equations," *Microw. Opt. Technol. Lett.,* vol. 48, no. 4, pp. 673-680, Apr. 2006.

[15] J. H. Lee and Q. H. Liu, "A 3-D spectral-element time-domain for electromagnetic simulation," *IEEE Trans. Microw. Theory Techn.,* vol. 55, no. 5, pp. 983-991, May 2007.

[16] O. A. Peverini, G. Addamo, G. Virone, R. Tascone, and R. Orta, "A spectral-element method for the analysis of 2-D waveguide devices with sharp edges and irregular shapes," *IEEE Trans. Microw. Theory Techn.,* vol. 59, no. 7, pp. 1685-1695, July 2011.

[17] J. Meixner, "The behavior of electromagnetic fields at edges," *IEEE Trans. Antennas Propag.,* vol. 20, no. 4, pp. 442-446, July 1972.

[18] A. Tibaldi, R. Orta, O. A. Peverini, G. Addamo, G. Virone, and R. Tascone, "A mortar-element method for the analysis of periodic structures," *International Conference on Electromagnetics in Advanced Applications (ICEAA), 2013,* pp. 117-120, 9-13 Sept. 2013.

[19] A. Tibaldi, R. Orta, O. A. Peverini, R. Tascone, G. Addamo, and G. Virone, "Analysis of diffraction gratings by the mortar-element method," *Numerical Electromagnetic Modeling and Optimization (NEMO),* 14-16 May 2014.

[20] L. B. Felsen and N. Marcuvitz, "Radiation and scattering of waves," John Wiley & Sons, Jan. 1994.

[21] P. P. Silvester and R. L. Ferrari, "Finite elements for electrical engineers," Cambridge University Press, Cambridge, 1996.

[22] R. Orta, S. Bastonero, and R. Tascone, "Numerical analysis of surface relief gratings," *Diffractive Optics and Optical Microsystems,* S. Martellucci and A. Chester Eds., pp. 47-56, Plenum Press, New York, USA, 1997.

[23] S. Bastonero, O. A. Peverini, R. Orta, and R. Tascone, "Anisotropic surface relief diffraction gratings under arbitrary plane wave incidence," *Optical and Quantum Electronics,* vol. 32, pp. 1013-1025, 2000

[24] S. A. Kemme, "Microoptics and nanooptics fabrication," CRC Press, Boca Raton, Florida, 2010.

Alberto Tibaldi (M'12) was born in Casale Monferrato, Italy, on February 21, 1987. In July 2009 and in November 2011 he received the B.Sc. and M.Sc degrees in Electronic Engineering (*summa cum laude*) from the Politecnico di Torino. In 2012 he joins the Applied Electromagnetics and Electronic Devices Group of the Istituto di Elettronica e di Ingegneria dell'Informazione e delle Telecomunicazioni (IEIIT) of the Consiglio Nazionale delle Ricerche (CNR) as Ph.D. student. From June to December 2013 he was a visiting member of the Terahertz Sensing Group, Delft University of Technology, Delft, The Netherlands. His scientific interests mainly regard the numerical simulation of electromagnetic passive devices.

Renato Orta (M'92-SM'99) received the Laurea degree in electronic engineering from the Politecnico di Torino, Turin, Italy in 1974. Since 1974, he has been a member of the Department of Electronics, Politecnico di Torino, initially as an Assistant Professor, then as an Associate Professor, and since 1999, as a Full Professor. In 1998, he was a Visiting Professor (CLUSTER Chair) with the Technical University of Eindhoven, Eindhoven, The Netherlands. He currently teaches courses on electromagnetic field theory and optical components. His research interests include the areas of microwave and optical components, radiation and scattering of electromagnetic and elastic waves, and numerical techniques.

Oscar Antonio Peverini (M'12) was born in Lisbon, Portugal, in 1972. He received the Laurea degree (*summa cum laudae*) in telecommunications engineering and the Ph.D. degree in electronic and communication engineering from the Politecnico di Torino, Turin, Italy, in 1997 and 2001, respectively. From August 1999 to March 2000, he was a Visiting Member with the Applied Physics/Integrated Optics Department, University of Paderborn, Paderborn, Germany. In February 2001, he joined the Istituto di Ricerca sull'Ingegneria delle Telecomunicazioni e dell'Informazione (IRITI), Consiglio Nazionale delle Ricerche (CNR), Turin, Italy. Since December 2001, he has been a Researcher with the Istituto di Elettronica e di Ingegneria Informatica e delle Telecomunicazioni (IEIIT), CNR. He teaches courses on electromagnetic field theory and applied mathematics at the Politecnico di Torino. His research interests include modeling, design, and measurement techniques of microwave passive devices and integrated acousto-optical components for communication and scientific equipment.

Giuseppe Addamo was born in Messina, Italy, in 1979. He received the Laurea degree (*summa cum laude*) in electronic engineering and Ph.D. degree in electronic and communication engineering from the Politecnico di Torino, Turin, Italy, in 2003 and 2007, respectively. In January 2007, he joined the Istituto di Elettronica e di Ingegneria dell'Informazione e delle Telecomunicazioni (IEIIT), Consiglio Nazionale delle Ricerche (CNR), Turin, Italy, as a Research Fellow, and in 2012, became a Researcher. He holds practical classes in courses on electromagnetic field theory and mathematical analysis at the Politecnico di Torino. His research interests are in the areas of microwave leaky antennas, dielectric radomes, high-power feed systems (e.g., orthomode transducers (OMTs), microwave filters), corrugated horns, frequency-selective surfaces, and large dielectric radomes.

Giuseppe Virone was born in Turin, Italy, in 1977. He received the Electronic Engineering degree (*summa cum laude*) and Ph.D. degree in electronic and communication engineering from the Politecnico di Torino, Turin, Italy, in 2001 and 2006, respectively. He is currently a Researcher with the Istituto di Elettronica e di Ingegneria Informatica e delle Telecomunicazioni (IEIIT), Consiglio Nazionale delle Ricerche (CNR), Turin, Italy. In 2002, he joined IEIIT as a Research Assistant. His research activities concern the design and numerical analysis of microwave and millimeter waveguide passive components for feed systems, antennas, frequency-selective surfaces, compensated dielectric radomes, and industrial applications.

Riccardo Tascone (M'03) was born in Genoa, Italy, in 1955. He received the Laurea degree (*summa cum laude*) in electronic engineering from the Politecnico di Torino, Turin, Italy, in 1980. From 1980 to 1982, he was with the Centro Studi e Laboratori Telecomunicazioni (CSELT), Turin, Italy, where his research mainly dealt with frequency-selective surfaces, waveguide discontinuities, and microwave antennas. In 1982, he joined the Centro Studi Propagazione e Antenne (CESPA) Consiglio Nazionale delle Ricerche (CNR), Turin, Italy, where he was initially a Researcher, and since 1991, a Senior Scientist (Dirigente di Ricerca). He has been Head of the Applied Electromagnetics Section of the Istituto di Ricerca sull'Ingeneria delle Telecomunicazioni e dell'Informazione (IRITI), an institute of CNR, Turin, Italy, and since September 2002, of the Istituto di Elettronica e di Ingegneria dell'Informazione e delle Telecomunicazioni (IEIIT), Turin, Italy, a newly established institute of CNR. He has held various teaching positions in the area of electromagnetics with the Politecnico di Torino. His current research activities are in the areas of microwave antennas, dielectric radomes, frequency-selective surfaces, radar cross section, waveguide discontinuities, microwave filters, multiplexers, optical passive devices, and radiometers for astrophysical observations.